Supporting Information

Enhanced Photoelectric Conversion Efficiency of Dye Sensitized Solar Cells by the Incorporation of One Dimension Luminescent $BaWO_4:Eu^{3+}$ Nanowires†

Yuping Wang[a], Yang Qu, Kai Pan, Guofeng Wang[a]*, and Yadong Li[b]

[a] *Key Laboratory of Functional Inorganic Material Chemistry, Ministry of Education, School of Chemistry and Materials Science, Heilongjiang University, Harbin, 150080, P. R. China*
Email: wanggf_w@163.com

[b] *Department of Chemistry and State Key Laboratory of New Ceramics and Fine Processing, Tsinghua University, Beijing, 100084, P. R. China*

1. Experimental procedure

Chemicals: Analytical grade $Ba(NO_3)_2$, $Eu(NO_3)_3 \cdot 6H_2O$, NaOH, Na_2WO_4, ethanol, and oleic acid were obtained from Beijing Chemical Reagents, China. The commercial TiO_2 powder (P25, Degussa, Germany) were purchased from standard source. The used Ru complex dye was cis-bis(isothiocyanato) bis (2,2′-bipyridyl-4,4′-dicarboxylato) ruthenium(II) bis-tetrabutylammonium (N719, Solaronix SA, Switzerland). The redox shuttle electrolyte was composed of 0.1M LiI (anhydrous, 99%, Acros), 0.05M I_2 (anhydrous, 99.8%), 0.5M tertbutylpyridine (99%, Aldrich), and 0.6M 1-propyl-2, 3-dimethylimidazolium iodide (99%) in acetonitrile (99%, Fluka). All of the reagents and solvents were used as received without further purification. Deionized water was used throughout.

For the synthesis of $BaWO_4$ nanocrystals: in a typical synthesis, 1 mL of Na_2WO_4 aqueous solution (1 mol/L) and 1 mmol of $Ba(NO_3)_2$ were added to a mixture of NaOH (1.2 g), ethanol (8 mL), deionized water (4 mL), and oleic acid (20 mL), and the solution was thoroughly stirred. Subsequently, the milky colloidal solution was transferred to a 50 mL Teflon-lined autoclave, and heated at 180 °C for 24 h. The systems were then allowed to cool to room temperature. The final products were collected by means of centrifugation, washed with ethanol, and finally dried in vacuum at room temperature. $BaWO_4$ nanocrystals doped with Eu^{3+} were prepared by the same procedure, except for adding additional $Eu(NO_3)_3$ into the solution at the initial stage.

Fabrication of photoelectrode and the assembly of DSSCs: several pastes, from homogeneously mixing $BaWO_4:Eu^{3+}$ and TiO_2 (Degussa P25) into 3 mL of TiO_2 colloid, were prepared with different concentrations of Eu^{3+}. The TiO_2 colloid was prepared following the previously published synthesis procedure.[1] A screen-printed double layer of TiO_2-$BaWO_4$: Eu^{3+} was used as the photoanode. A layer of TiO_2-$BaWO_4:Eu^{3+}$ was prepared by a doctor-blade method on the FTO substrate and then sintered at 450 °C for 1h. Subsequently, the second layer of TiO_2-$BaWO_4$: Eu^{3+} was covered on the first TiO_2-$BaWO_4$: Eu^{3+} film and then sintered at 450 °C for 30 min again. The thicknesses of all electrodes were determined to be around 10 μm (Figure S8). The sensitization of the photoelectrodes was achieved by immersing them into 0.34 mM $((C_4H_9)_4N)_2$[Ru(4-carboxy-4′-carboxylate-2,2′ bipyridine)$_2$$(NCS)_2$] dye (N719, Solaronix SA, Switzerland) in ethanol for 24h at room temperature. The Pt counter

electrodes were prepared following the previous literature.[2] The dye-sensitized photoelectrode and Pt counter electrode were adhered together with epoxy resin. The space between the electrodes was filled with the electrolyte, which comprised 0.6M 1-propyl-2,3-dimethyl-imidazolium iodide, 0.05M I_2, 0.1M LiI, and 0.5M tert-butylpyridine (TBP) in 3-methoxypropionitrile (3-MPN), by capillary action.

Characterization: The crystal structure was determined by a Rigaku (Japan) D/MAX-rA X-ray diffraction meter (XRD) equipped with graphite monochromatized Cu K α radiation (γ = 1.541874 Å), keeping the operating voltage and current at 40 kV and 40 mA. The size and morphology of the final products were investigated by scanning electron microscopy (SEM, Hitachi, S-4800) and transmission electron microscopy (TEM, JEOL, JEM-2010F). Dynamic light scattering (DLS) experiments were carried out on a Malvern Zetasizer (Nano-ZS, USA). The luminescence spectra were recorded with a Hitachi F-4600 fluorescence spectrophotometer (2.5 nm for spectral resolution (FWHM) of the spectrophotometer and 400 V for PMT voltage) at room temperature. The quantum yield of the down conversion was obtained by using a fluorescence detector (CDS610), an integrating sphere (CSTM-QE-060-SF), and a Xenon Lamp (500W, LS-500). The Raman spectra were measured by a HORIBA JOBIN YVON LabRam-HR 800 micro-Raman spectrometer.

Photocurrent-photovoltage curves were recorded by a BAS100B Electrochemical Analyzer. The power of the simulated light was calibrated to 100 mW/cm^{-2} by using a solar simulator radiometer (Oriel, USA). Photovoltaic measurements were carried out with a solar simulator (Oriel, USA) equipped with an AM 1.5G filter (Oriel, USA). The cell give an effective irradiation area of the working electrode of about 0.09cm^2.

2. Crystal Structure

The crystal structures and particle sizes of products were obtained by X-ray diffraction (XRD) patterns. Figure S3 shows the XRD patterns of $BaWO_4$:Eu^{3+} nanocrystals with different Eu^{3+} concentrations prepared at 180 °C for 24 h. The diffraction peaks can be indexed to the pure tetragonal phase $BaWO_4$ (JCPDS 43-0646). From the bottom to top in Fig. S3(a)-(j), the XRD patterns become broader and broader, suggesting that the crystalline size gradually decreased.

Figure S4 shows the Raman spectra of the characteristics of a scheelite tetragonal for the sagittate $BaWO_4$ with different Eu^{3+} concentration prepared at 180 °C for 24 h. Ba^{2+} are surrounded by eight oxygen atoms, and tungsten atoms are surrounded by four oxygen atoms in tetrahedral configuration to form $[WO_4]^{2-}$. The Raman bands for the internal modes centered at ~325, ~786, ~821, and ~919 cm^{-1} were observed. Figure S5 shows the IR spectra of $BaWO_4$ powders. The absorption peaks at ~813.18, ~1560.27, ~2852.92, ~2922.49 cm^{-1}. The antisymmetric stretching vibration $F_2(v_3)$ originating from the W-O in WO_4^{2-} tetrahedron corresponds to the broad intense peak at 813.18 cm^{-1}. The vibration at 1560.27 cm^{-1} is related to a COO- stretching mode for a bidentate complex. The absorption peaks appearing at 2922.49 cm^{-1} and 2852.92 cm^{-1} are the typical FT-IR absorption peaks of -CH_2- and -CH_3.[3,4]

3. Growth mechanism of $BaWO_4$ nanowires

Here, the nucleation and growth of $BaWO_4$ nanowires took place under nonequilibrium conditions. The growth process of $BaWO_4$ nanowires can be marked by Ostwald ripening: small crystals redissolve while larger crystals

grow by consumption of the solute species. We applied a diffusion-controlled kinetic model to explore the morphology evolution of nanowires. According to Xie and co-workers,[5] the growth rates of $BaWO_4$ nanowire in length and radial directions are only concentration-determined (Equation S1):

$$\begin{cases} g_1 = k_1[A]_0^{a_1} \\ g_2 = k_2[A]_0^{a2} \end{cases} \quad \text{(S1)}$$

Here, g_1 and g_2 are the growth rate in length and radial directions, which are time-independent. K_1 and K_2 are constants; $[A]_0$ is the starting $BaWO_4$ monomer concentration; $a_{1,2}$ can all be settled without influencing the qualitative result, since their deviations during the reaction are negligible.[5]

The relative growth rates of $BaWO_4$ nanowire in length and radial directions are given by Equations (S2)

$$\begin{cases} G_1 = g_1/L_1 \\ G_2 = g_2/L_2 \end{cases} \quad \text{(S2)}$$

Here, L_1 and L_2 are the longitudinal and side lengths of nanocrystals.

For a qualitative discussion, a_1 and a_2 are chosen to be $a_1 < a_2$. The following parameters are set: $a_1=1$, $a_2=2$, $K_1=2$, $K_2=1$.[5] As the starting monomer concentration $[A]_0$ is fixed initially, then in the case of $[A]_0=1$ mol/L (the initial concentration of Ba^{2+}/WO_4^{2-} ions was relatively low), $g_1>g_2$, which means $G_1>G_2$. Thus, the $BaWO_4$ nucleus forms nanowire by Ostwald ripening. While in the case of $[A]_0=3$ mol/L(the initial concentration of Ba^{2+}/WO_4^{2-} ions was relatively high), $g_1<g_2$, which means $G_1<G_2$. Thus, the $BaWO_4$ nucleus undergoes three dimension growth and forms $BaWO_4$ particles.[5]

In order to prove the growth mechanism, concentration-dependent experiments were carried out. The results indicated that three dimension $BaWO_4$ particles were obtained when the concentration of Ba^{2+}/WO_4^{2-} ions was high enough, as shown in Figure S2.

4. Photoluminescence of $BaWO_4$: Eu^{3+}

The $^5D_0 \rightarrow {}^7F_1$ transition is magnetic-dipole-allowed and its intensity is almost independent on the local environment around Eu^{3+} ions. The $^5D_0 \rightarrow {}^7F_2$ transition is electric-dipole-allowed due to an admixture of opposite parity $4f^{n-1}5d$ states by an odd parity crystal-field component. Therefore, its intensity is sensitive to the local structure around Eu^{3+} ions. The $^5D_0 \rightarrow {}^7F_3$ transition exhibits a mixed magnetic dipole and electric dipole character. The $^5D_0 \rightarrow {}^7F_4$ is an electric dipole transition. Figure S6 shown the corresponding excitation spectra of $BaWO_4$:Eu^{3+} with different Eu^{3+} concentrations. The broad band extending from 200 to 300 nm is assigned to the charge transfer transitions from the 2p orbital of O^{2-} to the 4f orbital of Eu^{3+}, which is related closely to the covalency between O^{2-} and Eu^{3+} and the coordination environment around Eu^{3+}. The sharp lines correspond to the f-f transitions of Eu^{3+} ions.

Reference for the supporting information

1. P. Wang, Q. Dai, S. Zakeeruddin, M. Forsyth, D. MacFarlane, M. Grätzel, *J. Am. Chem. Soc*., **2004**, *126*, 13590.
2. A. Hagfeldt, M. Grätzel, *Acc. Chem. Res*., **2000**, *33*, 269.
3. L. Burcham, E. Wachs, *Spect. Acta Part A*., **1998**, *54*, 1355.

4. F. Pontes, M. Maurera, A. Souza, E. Longo, E. Leite, R. Magnani, M. Machado, P. Pizani, J. Varela, *J. Eur. Ceram. Soc*., **2003**, *23*, 3001.
5. T. Xie, S. Li, Q. Peng, Y. Li, *Angew. Chem.*, **2009**, *121*, 202.

Figure S1. Growth mechanism of $BaWO_4$ nanocrystals.

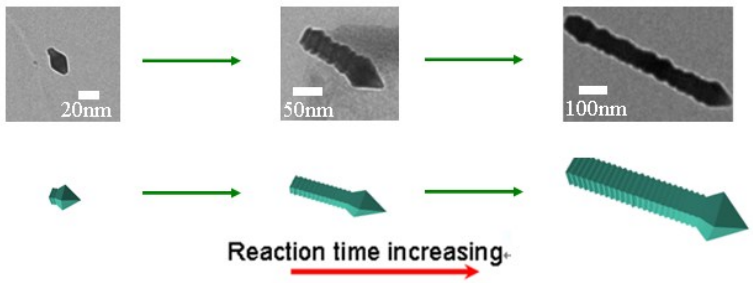

Figure S2. TEM images of $BaWO_4$ prepared at 180 °C for 24 h: 3 mol/L of Na_2WO_4 aqueous solution and a stoichiometric proportion of $Ba(NO_3)_2$ as raw materials.

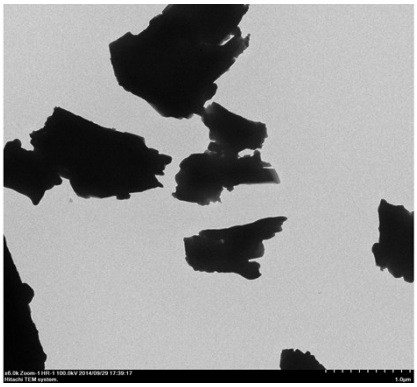

Figure S3. XRD patterns of (a) $BaWO_4$, (b) $BaWO_4$:1%Eu^{3+}, (c) $BaWO_4$:3%Eu^{3+}, (d) $BaWO_4$:5%Eu^{3+}, (e) $BaWO_4$:7%Eu^{3+}, (f) $BaWO_4$:10%Eu^{3+}, (g) $BaWO_4$:20%Eu^{3+}, (h) $BaWO_4$:30%Eu^{3+}, (i) $BaWO_4$:40%Eu^{3+}, and (j) $BaWO_4$:50%Eu^{3+} prepared at 180 °C for 24 h.

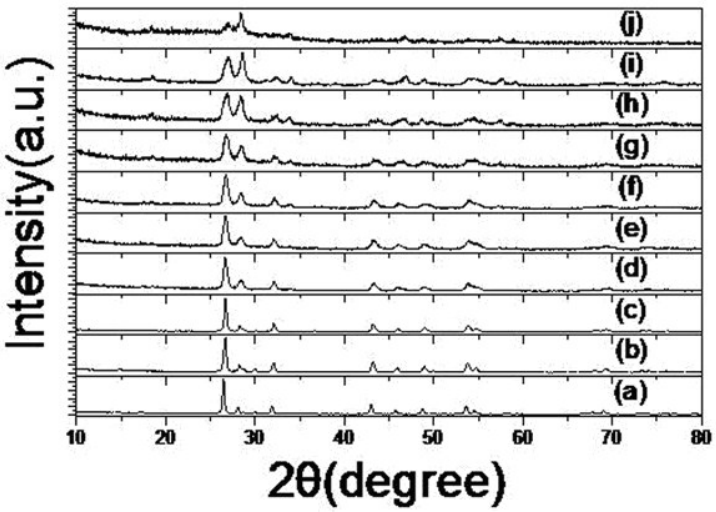

Figure S4. Dynamic light scattering (DLS) of $BaWO_4$: Eu^{3+} with different Eu^{3+} concentrations in cyclohexane.

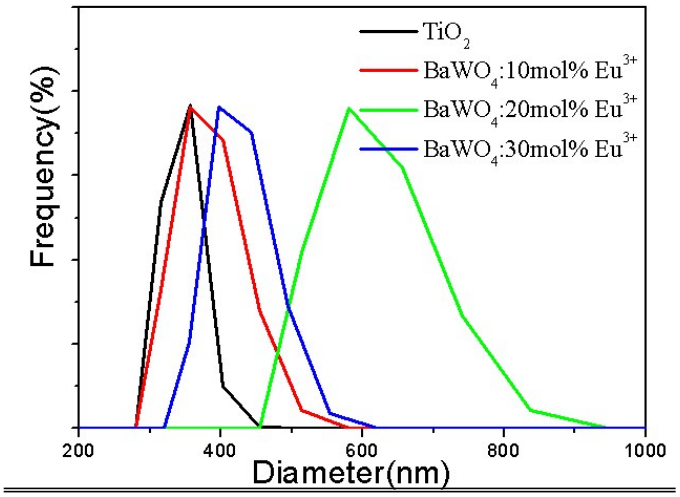

Figure S5. Raman spectra of (a) $BaWO_4$:1%Eu^{3+}, (b) $BaWO_4$:10%Eu^{3+}, (c) $BaWO_4$:30%Eu^{3+}, (d) $BaWO_4$:50%Eu^{3+} prepared at 180 °C for 24 h.

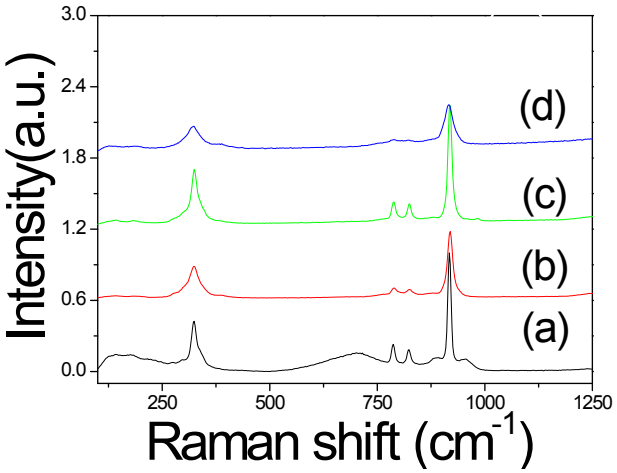

Figure S6. FT-IR spectra of $BaWO_4$ powders prepared at 180 °C for 24 h.

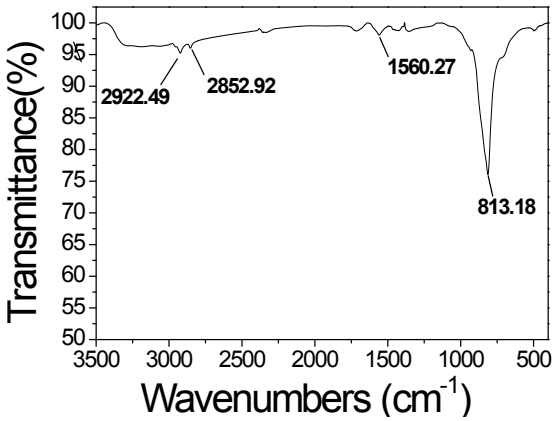

Figure S7. Excitation spectra of the $BaWO_4:Eu^{3+}$ nanocrystals with different Eu^{3+} concentrations monitored at 618 nm.

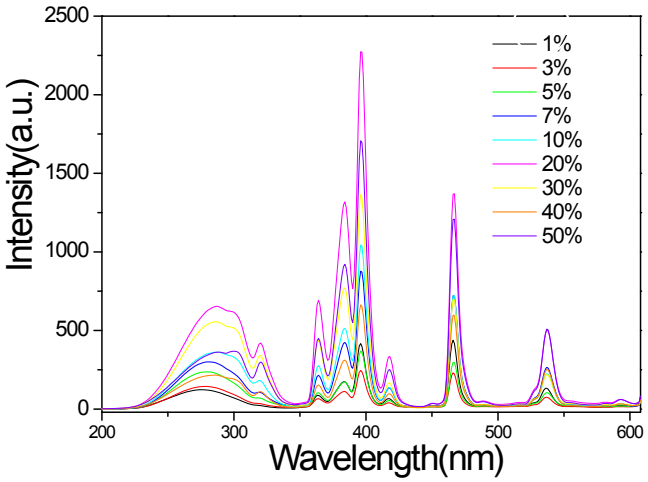

Figure S8. The thickness of each TiO_2 layer in the cells.

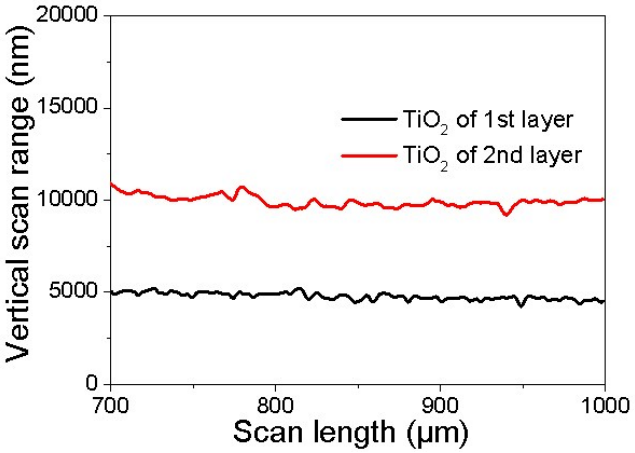

Figure S9. The luminescence spectra of the TiO_2-$BaWO_4$:Eu^{3+} photoanode before and after sensitization with N719 dye under 466 nm excitation.